Springer

KSME

Journal of Mechanical Science and Technology 31 (3) (2017) 1305~1313
www.springerlink.com/content/1738-494x(Print)/1976-3824(Online)
DOI 10.1007/s12206-017-0229-7

Green's-function-based-finite element analysis of fully plane anisotropic elastic bodies †

Hui Wang[1,2], Qing-Hua Qin[2,*] and Yong-Peng Lei[1]

[1]*Institute of Scientific and Engineering Computation, Henan University of Technology, Zhengzhou, 450001, China*
[2]*Research School of Engineering, Australian National University, Canberra, ACT 2601, Australia*

(Manuscript Received April 6, 2016; Revised October 8, 2016; Accepted October 30, 2016)

Abstract

In the paper, an anisotropic Green's function based hybrid finite element was developed for solving fully plane anisotropic elastic materials. In the present hybrid element, the interior displacement and stress fields were approximated by the linear combination of anisotropic Green's functions derived by Lekhnitskii formulation, the element frame fields were constructed by the interpolation of general shape functions widely used in the conventional finite element, and then they are linked by a new double-variable hybrid functional. Because the approximated interior fields exactly satisfied the governing equations related to anisotropic elasticity, all integrals in the present hybrid functional were performed along the element boundary and theoretically arbitrary hybrid polygonal element can be constructed. Finally, the present hybrid polygonal element with four edges was verified by making comparison of numerical results and exact solutions in a cantilever composite beam made with angled lamina.

Keywords: Anisotropy; Plane elasticity; Composites; Hybrid finite element; Green's functions

1. Introduction

Despite a large number of publications in the last decade, the accurate and efficient prediction of mechanical behavior of fully anisotropic materials like angled fiber/particle-reinforced composites, biomaterials, and so on, is still of great interest. However, compared to the experimental or analytical methods, resort to numerical techniques is usually necessary when treating complex geometries and loading conditions.

Among general computational techniques, the Finite element method (FEM) is still the one most extensively used in the analysis of anisotropic composite and engineering structures [1-3]. As an efficient alternative to the FEM, the Boundary element method (BEM), also commonly known as the Boundary integral equation (BIE) method, is also developed for solutions to those problems in anisotropic elasticity. For example, boundary element analysis of plane anisotropic bodies was conducted by Tan and Gao for investigating stress concentrations and cracks [4]. Pan and Amadei solved fracture mechanics problem of cracked plane anisotropic media with a new formulation of the BEM [5]. Qin and Mai solved problems of hole-crack interactions using BEM [6]. Similar analysis was performed by Wang and Sun for two-dimensional fracture analysis in anisotropic bodies [7].

In this study, a Green's function based hybrid finite element formulation different to the FEM and the BEM is formulated for two-dimensional elastic analysis in homogeneous fully anisotropic bodies. Early contributions to the development of the Green's function based hybrid finite element method include those for isotropic heat conduction [8], isotropic, plane elasticity with circular hole [9, 10] and orthotropic elastic analysis [11]. Due to the usage of Green's functions or fundamental solutions as kernels in the hybrid finite element formulation, the algorithm was named as HFS-FEM for simplicity. However, reports of its application to the case of general anisotropy have been extremely scarce indeed. So, herein we focus on the establishment of anisotropic Green's function based hybrid finite element formulation for two-dimensional anisotropy. It's worth noting that the work in Ref. [11] was just suitable for the orthotropic case in which the directions of material principal axes are the same as those of global coordinate axes. Otherwise, the full anisotropy will occur.

In the present computational model, the Green's functions or fundamental solutions are the analytical basis for constructing displacement and stress fields analytically satisfying the governing equations of problem within the element. Here, the Green's functions initially derived by Cruse [12] and latterly widely used in the BEM [5, 7, 13, 14] for the fully anisotropic elastic case are employed. Then, the independent element

*Corresponding author. Tel.: +61 6125 8274
E-mail address: qinghua.qin@anu.edu.au
† Recommended by Associate Editor Gang-Won Jang

frame displacement field is approximated by the conventional shape function interpolation, as done in the FEM [15, 16] and the BEM [17] for one-dimensional line elements. These two fields are connected by a double-variable hybrid functional to produce the finally force-displacement equations. Because of the inherent feature of Green's functions, the domain integral in the functional is removed and only integrals along the element boundary are remained. Therefore, the present method inherits the advantage of boundary integral in the BEM analysis and also it can provide versatile element material definition, like the FEM, which is important to perform multi-material analysis. So, the present computational method offers an efficient alternative to the FEM and the BEM.

The paper is organized as follows: Sec. 2 describes the basic equations for homogeneous general anisotropic elastic theory and Sec. 3 gives the corresponding Green's function expressions. In Sec. 4, the formulation of Green's function based hybrid finite element is establish and tested in Sec. 5 by several examples. Finally, some conclusions are drawn in Sec. 6.

2. Problem formulation

2.1 Plane anisotropic elastic governing equations

Before dealing with the development of the Green's function-based hybrid finite element formulation, it is useful to review some basic equations in two-dimensional homogeneous fully anisotropic elasticity. For this case, the governing equations including the strain-displacement relation, the constitutive relation and the equilibrium relation in the absence of body forces in a Cartesian coordinate system $\mathbf{x}=(X_1,X_2)$ can be given in matrix form as [18]

$$\begin{Bmatrix}\varepsilon_{11}\\ \varepsilon_{22}\\ \gamma_{12}\end{Bmatrix}=\begin{bmatrix}\partial_{,1} & 0\\ 0 & \partial_{,2}\\ \partial_{,2} & \partial_{,1}\end{bmatrix}\begin{Bmatrix}u_1\\ u_2\end{Bmatrix} \tag{1}$$

$$\begin{Bmatrix}\sigma_{11}\\ \sigma_{22}\\ \sigma_{12}\end{Bmatrix}=\begin{bmatrix}c_{11} & c_{12} & c_{16}\\ c_{12} & c_{22} & c_{26}\\ c_{16} & c_{26} & c_{66}\end{bmatrix}\begin{Bmatrix}\varepsilon_{11}\\ \varepsilon_{22}\\ \gamma_{12}\end{Bmatrix} \tag{2}$$

$$\begin{bmatrix}\partial_{,1} & 0 & \partial_{,2}\\ 0 & \partial_{,2} & \partial_{,1}\end{bmatrix}\begin{Bmatrix}\sigma_{11}\\ \sigma_{22}\\ \sigma_{12}\end{Bmatrix}=0 \tag{3}$$

where u_i , ε_{ij} and σ_{ij} $(i,j=1,2)$ are the plane components of displacement, strain and stress fields, respectively, and $\gamma_{12}=2\varepsilon_{12}$ is the engineering strain. The subscript comma represents the differential to the coordinate component, i.e. $\partial_{,i}=\partial/\partial X_i$, and c_{ij} $(i,j$=1,2,6) are elastic stiffness coefficients of the material.

Inversely, the stiffness matrix in the constitutive Eq. (2) can be expressed from the inverse of the generalized compliance matrix $\tilde{\mathbf{s}}$, that is

$$\mathbf{c}=\begin{bmatrix}c_{11} & c_{12} & c_{16}\\ c_{12} & c_{22} & c_{26}\\ c_{16} & c_{26} & c_{66}\end{bmatrix}=\begin{bmatrix}\tilde{s}_{11} & \tilde{s}_{12} & \tilde{s}_{16}\\ \tilde{s}_{12} & \tilde{s}_{22} & \tilde{s}_{26}\\ \tilde{s}_{16} & \tilde{s}_{26} & \tilde{s}_{66}\end{bmatrix}^{-1}=\tilde{\mathbf{s}}^{-1} \tag{4}$$

with

$$\tilde{s}_{ij}=\begin{cases}s_{ij} & \text{plane stress}\\ s_{ij}-s_{i3}s_{3j}/s_{33} & \text{plane strain}\end{cases}\quad (i,j=1,2,6) \tag{5}$$

where s_{ij} $(i,j=1,2,6)$ are elastic compliance coefficients of the material, which may be given in terms of engineering material constants as follows [18]

$$\begin{bmatrix}s_{11} & s_{12} & s_{16}\\ s_{12} & s_{22} & s_{26}\\ s_{16} & s_{26} & s_{66}\end{bmatrix}=\begin{bmatrix}1/E_1 & -\nu_{21}/E_2 & \eta_{1,12}/G_{12}\\ -\nu_{12}/E_1 & 1/E_2 & \eta_{2,12}/G_{12}\\ \eta_{12,1}/E_1 & \eta_{12,2}/E_2 & 1/G_{12}\end{bmatrix} \tag{6}$$

and

$$s_{i3}=-\frac{\nu_{i3}}{E_i}=-\frac{\nu_{3i}}{E_3},\ s_{33}=\frac{1}{E_3},\ s_{63}=\frac{\eta_{12,3}}{E_3}=\frac{\eta_{3,12}}{G_{12}} \tag{7}$$

where E_i is the Young's moduli referring to the axe X_i , G_{ij} is the shear modulus for the X_i-X_j plane, and ν_{ij} is the Poisson's ratio which is defined as the compressive strain in the X_j direction due to unit tension strain in the X_i direction. Also, $\eta_{ij,k}$ and $\eta_{k,ij}$ are the coefficients of mutual influence of the first and second kind, respectively, and they are zero in the case of specially orthotropic elastic materials.

Due to the symmetry of the matrix Eq. (6), the following relations exist

$$\begin{aligned}&E_1\nu_{21}=E_2\nu_{12},\quad E_3\nu_{i3}=E_i\nu_{3i}\\ &E_1\eta_{1,12}=G_{12}\eta_{12,1},\quad E_2\eta_{2,12}=G_{12}\eta_{12,2},\quad E_3\eta_{3,12}=G_{12}\eta_{12,3}\ .\end{aligned} \tag{8}$$

2.2 Coordinate transformation

Practically, the full anisotropy can be implemented by rotating the material principle axes of orthotropic laminate composite materials. Fig. 2 shows a typical coordinate rotation from the local coordinate axes (1,2) which are along the material principal directions E_1 and E_2 of orthotropic materials to the global coordinate axes (X_1,X_2). For this case, the compliance matrix Eq. (6) can be given by [19]

$$\begin{bmatrix}s_{11} & s_{12} & s_{16}\\ s_{12} & s_{22} & s_{26}\\ s_{16} & s_{26} & s_{66}\end{bmatrix}=\mathbf{R}\mathbf{T}^{-1}\mathbf{R}^{-1}\begin{bmatrix}1/E_1 & -\nu_{21}/E_2 & 0\\ -\nu_{12}/E_1 & 1/E_2 & 0\\ 0 & 0 & 1/G_{12}\end{bmatrix}\mathbf{T} \tag{9}$$

where θ is the material principle axis 1 orientation angle,

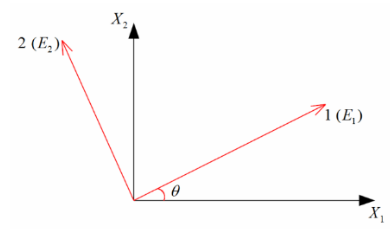

Fig. 1. Local and global coordinate axes.

$$R = \begin{bmatrix} 1 & 0 & 0 \\ 0 & 1 & 0 \\ 0 & 0 & 2 \end{bmatrix} \tag{10}$$

is the Reuter's matrix, and

$$T = \begin{bmatrix} \cos^2\theta & \sin^2\theta & \sin 2\theta \\ \sin^2\theta & \cos^2\theta & -\sin 2\theta \\ -\frac{1}{2}\sin 2\theta & \frac{1}{2}\sin 2\theta & \cos 2\theta \end{bmatrix} \tag{11}$$

is the transformation matrix.

Besides, appropriate boundary conditions should be complemented to keep the problems solvable, that is, on the boundary of the domain of interest, we have

$$\begin{Bmatrix} t_1 \\ t_2 \end{Bmatrix} = \begin{bmatrix} n_1 & 0 & n_2 \\ 0 & n_2 & n_1 \end{bmatrix} \begin{Bmatrix} \sigma_{11} \\ \sigma_{22} \\ \sigma_{12} \end{Bmatrix} = \begin{Bmatrix} \bar{t}_1 \\ \bar{t}_2 \end{Bmatrix} \tag{12}$$

and

$$\begin{Bmatrix} u_1 \\ u_2 \end{Bmatrix} = \begin{Bmatrix} \bar{u}_1 \\ \bar{u}_2 \end{Bmatrix} \tag{13}$$

where the overbar denotes the specified values.

3. The Green's functions for plane anisotropic elasticity

In the paper, a novel numerical method is developed to simulate the fully anisotropic plane elastic bodies and Green's functions or fundamental solutions play an important role in the present numerical method. In order to keep the paper complete, the anisotropic plane elastic Green's functions or fundamental solutions are given in this section.

By introducing Airy's stress functions, Lekhnitskii has shown that the characteristic equation for a homogeneous fully anisotropic elastic material is [18]

$$\tilde{s}_{11}\mu^4 - 2\tilde{s}_{16}\mu^3 + \left(2\tilde{s}_{12} + \tilde{s}_{66}\right)\mu^2 - 2\tilde{s}_{26}\mu + \tilde{s}_{22} = 0\,. \tag{14}$$

Through a consideration of potential energy, Lekhnitskii has shown that the characteristic equation has no real roots and the roots are always distinct as long as the material is not isotropic. Thus, for a generally anisotropic body the roots of the characteristic equation are always complex and are of the form

$$\mu_i = \alpha_i + \beta_i \mathrm{I}, \qquad \bar{\mu}_i = \alpha_i - \beta_i \mathrm{I} \quad (i=1,2) \tag{15}$$

where $\mathrm{I} = \sqrt{-1}$, α_i, β_i are real constants and $\beta_i > 0$ from thermodynamic considerations.

Subsequently, the characteristic directions may be denoted by [20, 21]

$$z_\alpha = X_1 + \mu_\alpha X_2 \qquad (\alpha = 1,2) \tag{16}$$

and their complex conjugates. (X_1, X_2) is an arbitrary field point in the domain.

In order to express the fundamental solutions, another two complex variables related to source points can be expressed as

$$z_\alpha^s = X_1^s + \mu_\alpha X_2^s \qquad (\alpha = 1,2) \tag{17}$$

where (X_1^s, X_2^s) is the corresponding source point.

Then the induced displacement components along the 1- and 2- directions at the field point (X_1, X_2) due to a unit concentrated force along the k- direction (k=1,2) at the source point (X_1^s, X_2^s) can be written as [5, 7, 12, 13]

$$\begin{aligned} u_{k1}^*\left(z_\alpha, z_\alpha^s\right) &= 2\,\mathrm{Re}\left\{\sum_{\alpha=1}^{2} A_{k\alpha} P_{1\alpha} \ln\left(z_\alpha - z_\alpha^s\right)\right\} \\ u_{k2}^*\left(z_\alpha, z_\alpha^s\right) &= 2\,\mathrm{Re}\left\{\sum_{\alpha=1}^{2} A_{k\alpha} P_{2\alpha} \ln\left(z_\alpha - z_\alpha^s\right)\right\} \end{aligned} \tag{18}$$

where Re means the real part of any complex expression, and

$$\begin{Bmatrix} P_{1\alpha} \\ P_{2\alpha} \end{Bmatrix} = \begin{Bmatrix} \tilde{s}_{11}\mu_\alpha^2 + \tilde{s}_{12} - \tilde{s}_{16}\mu_\alpha \\ \tilde{s}_{12}\mu_\alpha + \tilde{s}_{22}/\mu_\alpha - \tilde{s}_{26} \end{Bmatrix} \qquad (\alpha = 1,2)\,. \tag{19}$$

Also in Eq. (18), the complex constants $A_{k\alpha}$ can be obtained from the requirements of unit load at the source point and displacement continuity for the fundamental solutions, by the solution of the linear system

$$\begin{bmatrix} 1 & -1 & 1 & -1 \\ \mu_1 & -\bar{\mu}_1 & \mu_2 & -\bar{\mu}_2 \\ P_{11} & -\bar{P}_{11} & P_{12} & -\bar{P}_{12} \\ P_{21} & -\bar{P}_{21} & P_{22} & -\bar{P}_{22} \end{bmatrix} \begin{Bmatrix} A_{k1} \\ \bar{A}_{k1} \\ A_{k2} \\ \bar{A}_{k2} \end{Bmatrix} = \frac{1}{2\pi \mathrm{I}} \begin{Bmatrix} \delta_{k2} \\ -\delta_{k1} \\ 0 \\ 0 \end{Bmatrix}, \quad (k = 1,2) \tag{20}$$

where $\delta_{k\alpha}$ denotes the Kronecker Dirac function, and $\mathrm{I} = \sqrt{-1}$ is the unit pure imaginary number.

It is necessary to note that for the case of isotropic material, the roots of characteristic equation are pure imaginary I and $-\mathrm{I}$, which lead to the coefficient matrix of the linear system Eq. (20) singular. Because this, it is not possible to directly use Eq. (20) with the isotropic formulation.

Furthermore, the Green's strain, stress and traction kernels can be derived by the strain-displacement relation Eq. (1), the anisotropic stress-strain constitutive Eq. (2) and the traction-stress relation Eq. (12), respectively.

4. Hybrid finite element formulation

In the absence of body forces, the hybrid variational functional for an particular anisotropic plane elastic element can be written as [9, 11, 22]

$$\Pi_{me} = \int_{\Omega_e} \frac{1}{2}\sigma_{ij}\varepsilon_{ij}\mathrm{d}\Omega - \int_{\Gamma_e^\sigma} \bar{t}_i\tilde{u}_i\mathrm{d}\Gamma + \int_{\Gamma_e} t_i\left(\tilde{u}_i - u_i\right)\mathrm{d}\Gamma \tag{21}$$

where u_i and $\tilde{u}_i$ are independent displacement fields defined in the interior of element and on the element boundary. For example, in the presented approach, the interior displacement field $\mathbf{u} = \{u_1, u_2\}^{\mathrm{T}}$ can be defined by means of the linear combination of the corresponding fundamental solutions given by Eq. (18) at n_s source points, i.e.

$$\mathbf{u}(\mathbf{x}) = \mathbf{N}\mathbf{c}_e \tag{22}$$

with

$$\mathbf{N} = \begin{bmatrix} u_{11}^*(\mathbf{x},\mathbf{y}_1) & u_{21}^*(\mathbf{x},\mathbf{y}_1) & \cdots & u_{11}^*(\mathbf{x},\mathbf{y}_{n_s}) & u_{21}^*(\mathbf{x},\mathbf{y}_{n_s}) \\ u_{12}^*(\mathbf{x},\mathbf{y}_1) & u_{22}^*(\mathbf{x},\mathbf{y}_1) & \cdots & u_{12}^*(\mathbf{x},\mathbf{y}_{n_s}) & u_{22}^*(\mathbf{x},\mathbf{y}_{n_s}) \end{bmatrix} \tag{23}$$
$$\mathbf{c}_e = \left\{c_1^1 \quad c_2^1 \; \vdots \cdots \vdots \; c_1^{n_s} \quad c_2^{n_s}\right\}^{\mathrm{T}}.$$

It's evident that Eq. (22) *prior* satisfies the governing equations in terms of displacements if a series of source points $\mathbf{y}_k$ $(k = 1 \to n_s)$ are placed outside the element by the following simple rule [9, 22]

$$\mathbf{y}_k = \mathbf{x}_b + \gamma(\mathbf{x}_b - \mathbf{x}_c) \tag{24}$$

which can produce boundary geometrically similar to the physical element boundary. In Eq. (24), γ is a dimensionless coefficient controlling the distance of the source point and the element boundary, $\mathbf{x}_b$ is the elementary boundary point, i.e. node, and $\mathbf{x}_c$ the geometrical centroid of the element. Investigation of the effect of the parameter γ has been fully discussed for isotropic and orthotropic elastic problems [9, 11], and it was found that there is a large interval to choose the parameter γ to achieve relatively stable numerical results. In this study, $\gamma = 5$ is used, unless stated otherwise.

As a consequence, the stress approximation $\boldsymbol{\sigma} = \{\sigma_{11}, \sigma_{22}, \sigma_{12}\}^{\mathrm{T}}$ can be given by combining of Green's stress kernels with unknown source intensities, that is,

$$\boldsymbol{\sigma}(\mathbf{x}) = \mathbf{T}\mathbf{c}_e \tag{25}$$

where

$$\mathbf{T} = \begin{bmatrix} \sigma_{111}^*(\mathbf{x},\mathbf{y}_1) & \sigma_{211}^*(\mathbf{x},\mathbf{y}_1) & \cdots & \sigma_{111}^*(\mathbf{x},\mathbf{y}_{n_s}) & \sigma_{211}^*(\mathbf{x},\mathbf{y}_{n_s}) \\ \sigma_{122}^*(\mathbf{x},\mathbf{y}_1) & \sigma_{222}^*(\mathbf{x},\mathbf{y}_1) & \cdots & \sigma_{122}^*(\mathbf{x},\mathbf{y}_{n_s}) & \sigma_{222}^*(\mathbf{x},\mathbf{y}_{n_s}) \\ \sigma_{112}^*(\mathbf{x},\mathbf{y}_1) & \sigma_{212}^*(\mathbf{x},\mathbf{y}_1) & \cdots & \sigma_{112}^*(\mathbf{x},\mathbf{y}_{n_s}) & \sigma_{212}^*(\mathbf{x},\mathbf{y}_{n_s}) \end{bmatrix}. \tag{26}$$

On the other hand, the frame displacement field $\tilde{\mathbf{u}} = \{\tilde{u}_1, \tilde{u}_2\}^{\mathrm{T}}$ defined on the element boundary is assumed to be same as the shape functions used in the boundary element method and finite element method, that is,

$$\tilde{\mathbf{u}}(\mathbf{x}) = \tilde{\mathbf{N}}\mathbf{d}_e \tag{27}$$

where $\mathbf{d}_e$ denotes the element nodal DOF and $\tilde{\mathbf{N}}$ represents shape functions matrix.

Appling the Gaussian theorem again to the above functional and considering the natural satisfaction of the equilibrium equation under the assumed displacement and stress fields inside the element, we have the final expression for the present HFS finite element model

$$\Pi_{me} = -\frac{1}{2}\int_{\Gamma_e} t_i u_i \mathrm{d}\Gamma - \int_{\Gamma_e^\sigma} \bar{t}_i\tilde{u}_i\mathrm{d}\Gamma + \int_{\Gamma_e} t_i\tilde{u}_i\mathrm{d}\Gamma. \tag{28}$$

Substituting Eqs. (22) and (27) into the simplified functional Eq. (28) produces

$$\Pi_{me} = -\frac{1}{2}\mathbf{c}_e^{\mathrm{T}}\mathbf{H}_e\mathbf{c}_e - \mathbf{d}_e^{\mathrm{T}}\mathbf{g}_e + \mathbf{c}_e^{\mathrm{T}}\mathbf{G}_e\mathbf{d}_e \tag{29}$$

in which

$$\mathbf{H}_e = \int_{\Gamma_e} \mathbf{Q}^{\mathrm{T}}\mathbf{N}\mathrm{d}\Gamma,\ \ \mathbf{G}_e = \int_{\Gamma_e} \mathbf{Q}^{\mathrm{T}}\tilde{\mathbf{N}}\mathrm{d}\Gamma,\ \ \mathbf{g}_e = \int_{\Gamma_e^\sigma} \tilde{\mathbf{N}}^{\mathrm{T}}\bar{\mathbf{t}}\mathrm{d}\Gamma \tag{30}$$

with

$$\mathbf{Q} = \begin{bmatrix} n_1 & 0 & n_2 \\ 0 & n_2 & n_1 \end{bmatrix}\mathbf{T}. \tag{31}$$

In Eq. (30), the matrices $\mathbf{H}_e$ and $\mathbf{G}_e$ are performed along the element boundary. Practically, they can be numerically integrated by Gaussian integration edge by edge. The detailed evaluation procedure is similar to that in the Trefftz FEM [23], in which the computing code was provided for reference.

To enforce inter-element continuity on the common element boundary, the unknown vector $\mathbf{c}_e$ should be expressed in terms of nodal DOF $\mathbf{d}_e$. The minimization of the functional Π_{me} with respect to $\mathbf{c}_e$ and $\mathbf{d}_e$, respectively, yields

$$\begin{aligned} &\partial\Pi_{me}/\partial\mathbf{c}_e^{\mathrm{T}} = -\mathbf{H}_e\mathbf{c}_e + \mathbf{G}_e\mathbf{d}_e = \mathbf{0} \\ &\partial\Pi_{me}/\partial\mathbf{d}_e^{\mathrm{T}} = \mathbf{G}_e^{\mathrm{T}}\mathbf{c}_e - \mathbf{g}_e = \mathbf{0} \end{aligned} \tag{32}$$

from which we can obtain the element stiffness equation

$$\mathbf{K}_e \mathbf{d}_e = \mathbf{g}_e \tag{33}$$

and the relationship of $\mathbf{c}_e$ and $\mathbf{d}_e$

$$\mathbf{c}_e = \mathbf{H}_e^{-1} \mathbf{G}_e \mathbf{d}_e \ . \tag{34}$$

In Eq. (33), the element stiffness matrix is expressed as

$$\mathbf{K}_e = \mathbf{G}_e^{\mathrm{T}} \mathbf{H}_e^{-1} \mathbf{G}_e \ . \tag{35}$$

From the derivation procedure, it can be seen that the advantage of the present hybrid finite element formulation is in fact that the element interior displacement and stress fields have analytically satisfied the anisotropic elastic equations. Therefore, the present element can produce more accurate numerical results, which have been shown by Wang and Qin for homogeneous/inhomogeneous isotropic elasticity [9, 10]. Besides, the feature of element boundary integrals make us construct versatile convex polygonal elements, instead of conventional triangular and quadrilateral elements [9, 22].

5. Numerical results

In this section, several examples including bending of a cantilever beam, stress concentration along a circular hole, and biomechanical analysis in human femur bone are studied to illustrate the performance of the present method. All examples are under the plane stress condition, except for special statement. Certainly, the plane strain analysis can also be carried out by the present method if the material compliance coefficients in Eq. (5) can be provided completely.

5.1 Bending problem of a cantilever beam

This example is used to check the accuracy and effectiveness of the present Green's-function-based hybrid finite element. A cantilever beam made with angled boron/epoxy lamina is here taken into consideration. The length of the beam is $l = 350$ mm, and the height and width of the rectangular cross-section are $b = 50$ mm and $h = 1$ mm, respectively. The uniform pressure $q = 2$ MPa is applied to the top edge of the beam, as shown in Fig. 2. The symbol θ appeared in the figure denotes the angle between the local orthotropic material principal direction 1 parallel to the fibers and the global coordinate axis X_1. The material properties in the principal directions for the orthotropic unidirectional boron/epoxy panel are given by [24]

$$E_1 = 113 \text{ GPa}, \quad E_2 = 52.7 \text{ GPa},$$
$$G_{12} = 28.5 \text{ GPa}, \quad \nu_{12} = 0.45 \ .$$

With the plane stress assumption, the analytical solutions of displacements and stresses are given in the appendix for the purpose of comparison. Firstly, the convergence of the present anisotropic hybrid elements is investigated. For this purpose, two different mesh configurations respectively including 20 and 80 hybrid finite elements are shown in Fig. 3 and numerical results of the deflection u_2 and the stress component σ_{11} at specified locations are listed in Table 1, from which it's evidently found that the numerical results of both the displacement and the stress results are closer to the exact solutions as the number of elements increases. So the convergence of the present element is demonstrated. Additionally, as a simple illustration of the influence of the parameter γ, which controls the distance of source point to the element boundary, Table 2 indicates the variation of σ_{11} at the specified location (175 mm, -25 mm) for different γ for the case of 80 hybrid finite elements and $\theta = 0$. We observe from Table 2 that there is a large interval to choose the parameter γ to produce relatively stable results, and similar discuss can be found in Refs. [9, 11].

Next, the effect of the fiber rotation angle θ is investigated by means of the present anisotropic elements. During the computation, 80 hybrid finite elements with 289 nodes are employed to evaluate the variations of the vertical displacement (deflection) u_2 on the horizontal line $X_2 = 0$ and the

Table 1. Convergence of the present hybrid finite element for the case $\theta = 0$.

	HFS-FEM		EXACT
	20 elements	80 elements	
u_2 (mm) at (0,0)	3.2830 (2.02 %)	3.2851 (1.95 %)	3.3507
σ_{11} (MPa) at (175 mm, -25 mm)	73.036 (0.204 %)	72.868 (0.026 %)	72.887

Table 2. Variation of σ_{11} with different γ for the case of 80 hybrid finite elements and $\theta = 0$.

γ	2	3	4	5	6	7	8
σ_{11} (MPa)	71.653	72.716	72.829	72.868	72.884	72.891	72.894

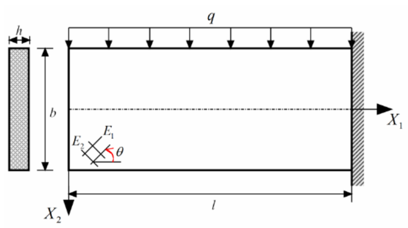

Fig. 2. Cantilever beam made with angled boron/epoxy lamina.

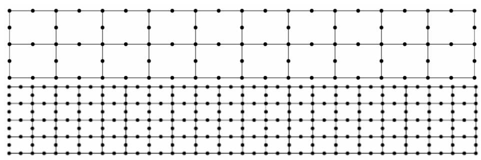
Fig. 3. Mesh configurations with 20 (upper) and 80 (below) hybrid finite elements.

Table 3. Results of the displacement at (0,0) and the stress at (175 mm, -25 mm) for different fiber orientations.

θ	EXACT		HFS-FEM	
	u_2 (mm)	σ_{11} (MPa)	u_2 (mm)	σ_{11} (MPa)
0°	3.3507	72.887	3.2851	72.868
30°	4.2108	78.385	4.1233	78.299
60°	6.0352	77.113	5.9428	77.033
90°	6.9975	73.214	6.9228	73.417

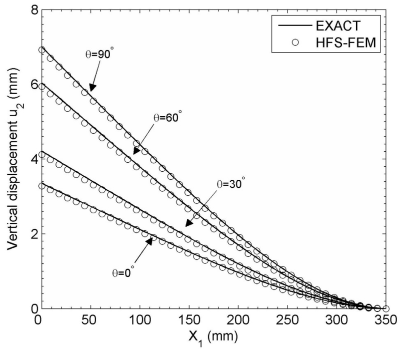

Fig. 4. Displacement variations along the horizontal line $X_2 = 0$ of the beam for the boron/epoxy composite.

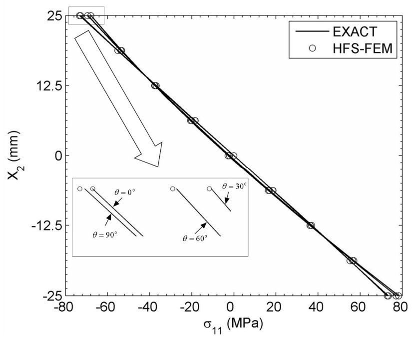

Fig. 5. Stress distributions along the vertical line $X_1 = l/2$ of the beam for the boron/epoxy composite.

stress component σ_{11} along the vertical line $X_1 = l/2$, and numerical results are displayed in Figs. 4 and 5. On the one hand, it's observed that there is good agreement between the numerical results and the exact solutions of both the displacement and the stress, so the performance of the present elements is demonstrated again. On the other hand, we observe that there is a remarkable increase of the deflection of the beam when the value of θ becomes large, while the variation of stress results is slight. Furthermore, Fig. 5 clearly shows an approximated linear change of the normal stress σ_{11} and the positive sign in Fig. 5 indicates the normal stress is tensile while the negative sign indicates the regions in which this stress is compressive, as desired. Finally, results of the vertical displacement and the stress component at two key points (0, 0) and (175 mm, -25 mm) for different fiber orientations are tabulated in Table 3, from which the good agreement is obviously observed between results from the present method and exact solutions.

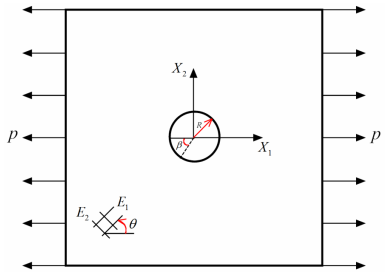

Fig. 6. Sketch of a circular hole in an anisotropic square plate with uniform tension in the horizontal direction.

5.2 Stress concentration problem in a square plate with circular hole

The second example is presented to investigate stress concentration in an infinite plate containing a circular hole under remote uniform tension p in the X_1 direction, as shown in Fig. 6. This problem provides an excellent example to illustrate the modelling efficiency of the present hybrid finite element formulation, particularly for treating the curved hole boundary around which the stresses also vary very rapidly.

In the computational treatment, the radius of the circle is taken to be 1 mm, and a considerable distance is chosen from the circular opening to be a finite square sheet, i.e. with side length 20 mm, to approximately replace the infinite domain so that the effects of the finite boundaries would not be significant. The uniform tension $p = 100$ MPa. The analysis was carried out for the orthotropic graphite-epoxy material described by the following four independent engineering elastic constants in the principal directions [4]

$$E_1 = 181 \text{ GPa}, \quad E_2 = 10.3 \text{ GPa},$$
$$G_{12} = 7.17 \text{ GPa}, \quad \nu_{12} = 0.28,$$

which can be used to sufficiently define a fully anisotropic material by setting different fiber orientation angle θ. Also, we find that the graphite-epoxy material in this example has stronger anisotropy than the boron/epoxy material mentioned in example 1, because $E_1/E_2 = 17.57$, $E_1/G_{12} = 25.24$ for the graphite-epoxy material and $E_1/E_2 = 2.14$, $E_1/G_{12} = 3.96$ for the boron/epoxy material.

It should perhaps be noted that the entire physical domain is modeled here, because, even though there are planes of symmetry for the geometry and load conditions, no such symmetry exists for the material properties. In the practical computation, the computational mesh shown in Fig. 7 is employed to model the entire domain, in which 256 8-node elements with 832 nodes are included. Fig. 8 shows the scaled variation of the normalized tangential stress, σ_β / p, around the circumference of the circular hole for the case of material orientation angle $\theta = 0$. To demonstrate the efficiency of the present Green's function-based hybrid finite element, the numerical

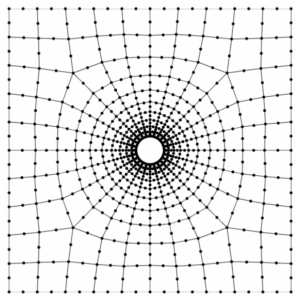

Fig. 7. Mesh configuration for the stress concentration problem.

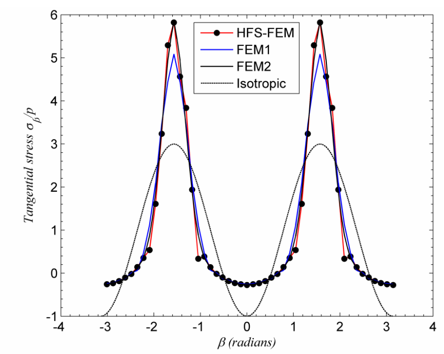

Fig. 8. Tangential stress around the circumference of the circular hole for zero material orientation angle.

results from the conventional FEM implemented in ABAQUS are provided to make comparison. In ABAQUS, two mesh discretisations are produced. The first one (FEM1) is same as that used in the present method, while the second one (FEM2) is relatively refined mesh by using more elements and nodes (1024 elements and 3200 nodes). It's found in Fig. 8 that the present method with the mesh discretization involving less numbers of elements can produce almost same accurate results as those from the conventional FEM which uses a refined mesh discretization. Additionally, the stress concentration factor can be evaluated by the ratio of maximum hoop stress $\sigma_\beta^{\max}$ and the average stress p and for the case of zero material orientation angle, it has values of 5.8209 (HFS-FEM), 5.0883 (FEM1) and 5.8548 (FEM2), respectively. Furthermore, it can be seen that the anisotropy causes a qualitatively quite different and rapid variation of the tangential stress along the periphery of the hole, compared to the isotropic case, which has a theoretical value 3 of the stress concentration factor.

In order to investigate the effect of material orientation angle θ on the tangential stress around the circular hole, Figs. 9 and 10 respectively give the variations of the the normalized tangential stress σ_β and the stress concentration factor $\sigma_\beta^{\max}/p$ for various material orientation angles. It's evident from Fig. 9 that dramatic change of the distribution of tangential stress σ_β is led by the material orientation angle θ, and Fig. 10 shows that the maximum tangential stress decreases with the increase of material orientation angle.

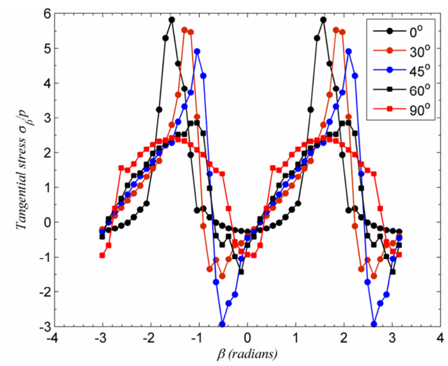

Fig. 9. Tangential stress around the circumference of the circular hole under tension for various material orientation angles.

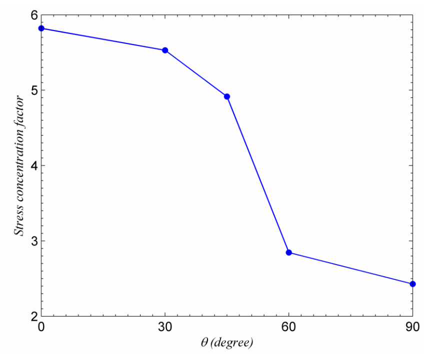

Fig. 10. Variation of stress concentration factor for various material orientation angles.

5.3 Biomechanical problem in anisotropic bone model

In the last example, the two-dimensional simplified anisotropic human femoral bone model is considered. The engineering elastic constants along the material principal directions are given by [25]

$$E_1 = 17 \text{ GPa}, \quad E_2 = 11.5 \text{ GPa},$$
$$G_{12} = 3.3 \text{ GPa}, \quad \nu_{12} = 0.31 .$$

During the computation, it's assumed that the right upper surface of the bone model shown in Fig. 11 is subjected to a uniform pressure 10 MPa. The bottom of the bone model is fixed by constraint of the displacements along the two coordinate axis directions. Total 731 elements with 2286 nodes are employed to discretize the model, as shown in Fig. 11. Due to the bending caused by the specified pressure on the right upper surface, it is inevitably that the stress, especially the normal stress σ_{22}, has a strong variation on the bottom surface which is fixed. To display this, Fig. 12 plots the variation of the normal stress σ_{22} on the bottom edge. It can be seen that the stress component σ_{22} changes from tensile stress (positive sign) to compressive stress (negative sign), as we expected. Additionally, the numerical results from the conventional FEM implemented by ABAQUS are provided in Fig. 12, and a good agreement between results from the present

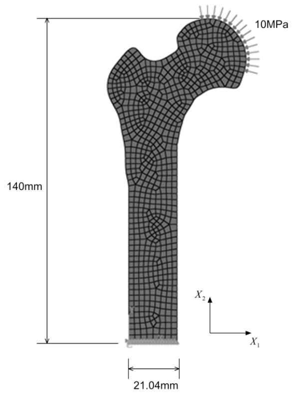

Fig. 11. Two-dimensional anisotropic human femoral bone model.

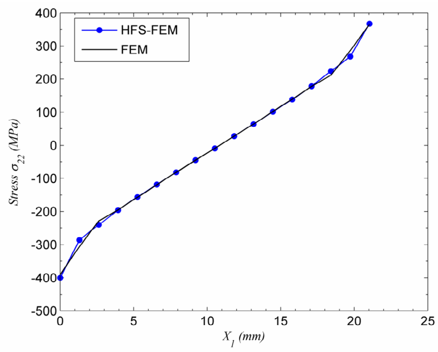

Fig. 12. Variation of the normal stress σ_{22} on the bottom surface.

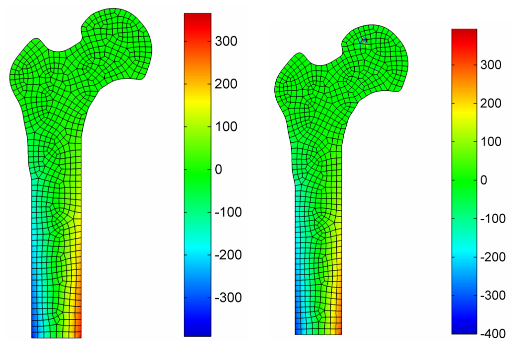

Fig. 13. Contour maps of the normal stress component σ_{22} for the FEM (left) and the present method (right).

method and the conventional FEM is observed. Finally, the stress distribution of σ_{22} by the present method in the entire bone structure is plotted in Fig. 13, and simultaneously the FEM results are plotted in the figure for comparison. Again, a good agreement is observed between the results from the conventional FEM and the present method.

6. Conclusions

In the paper, a Green's function based hybrid finite element method using the quadratic hybrid element formulation is successfully implemented for solving two-dimensional homogeneous fully anisotropic elastic problems. The displacement and stress Green's function expressions employed here are based on the Lekhnitskii potential method. The convergence and numerical accuracy of this numerical method are demonstrated with a number of problems involving anisotropic beam bending, stress concentration caused by a circular cut in infinite anisotropic media and biomechanical problem in anisotropic bone model. Numerical solutions computed in the present study are shown to be in excellent agreement with the analytical solutions or those from the conventional FEM, even with the relatively modest number of elements used.

Acknowledgment

The work described in this paper was partially supported by the National Natural Science Foundation of China (No. 11372100, 11472099) and the Program for Innovation Talents of Science and Technology in Universities in Henan Province (No. 13HASTIT019).

References

[1] E. Carrera, Theories and finite elements for multilayered, anisotropic, composite plates and shells, *Archives of Computational Methods in Engineering*, 9 (2) (2002) 87-140.
[2] A. M. O'Mahony, J. L. Williams and P. Spencer, Anisotropic elasticity of cortical and cancellous bone in the posterior mandible increases peri-implant stress and strain under oblique loading, *Clinical Oral Implants Research*, 12 (6) (2001) 648-657.
[3] Q. H. Qin, Hybrid-Trefftz finite element method for Reissner plates on an elastic foundation, *Computer Methods in Applied Mechanics and Engineering*, 122 (3) (1995) 379-392.
[4] C. L. Tan and Y. L. Gao, Boundary element analysis of plane anisotropic bodies with stress concentrations and cracks, *Composite Structures*, 20 (1) (1992) 17-28.
[5] E. Pan and B. Amadei, Fracture mechanics analysis of cracked 2-D anisotropic media with a new formulation of the boundary element method, *International Journal of Fracture*, 77 (2) (1996) 161-174.
[6] Q. H. Qin and Y. W. Mai, BEM for crack-hole problems in thermopiezoelectric materials, *Engineering Fracture Mechanics*, 69 (5) (2002) 577-588.
[7] Y. B. Wang and Y. Z. Sun, A new boundary integral equation method for cracked 2-D anisotropic bodies, *Engineering Fracture Mechanics*, 72 (13) (2005) 2128-2143.
[8] H. Wang and Q. H. Qin, Hybrid FEM with fundamental solutions as trial functions for heat conduction simulation, *Acta Mechanica Solida Sinica*, 22 (5) (2009) 487-498.
[9] H. Wang and Q. H. Qin, Fundamental-solution-based hybrid FEM for plane elasticity with special elements, *Computational Mechanics*, 48 (5) (2011) 515-528.
[10] H. Wang and Q. H. Qin, Boundary integral based graded element for elastic analysis of 2D functionally graded plates, *European Journal of Mechanics-A/Solids*, 33 (2012) 12-23.

[11] H. Wang and Q. H. Qin, Fundamental-solution-based finite element model for plane orthotropic elastic bodies, *European Journal of Mechanics-A/Solids*, 29 (5) (2010) 801-809.

[12] T. A. Cruse, *Boundary element analysis in computational fracture mechanics,* Kluwer Academic Publisher, Dordrecht (1988).

[13] P. Sollero and M. H. Aliabadi, Fracture mechanics analysis of anisotropic plates by the boundary element method, *International Journal of Fracture*, 64 (4) (1993) 269-284.

[14] Q. H. Qin, *Green's function and boundary elements of multifield materials,* Elsevier, Oxford (2007).

[15] O. C. Zienkiewicz and R. L. Taylor, *The finite element method: Solid mechanics*, Fifth Edition, Butterworth-Heinemann, Oxford (2000).

[16] Q. H. Qin, Solving anti-plane problems of piezoelectric materials by the Trefftz finite element approach, *Computational Mechanics*, 31 (6) (2003) 461-468.

[17] P. K. Banerjee and R. Butterfield, *Boundary element methods in engineering science,* McGraw-Hill, London (1981).

[18] S. G. Lekhnitskii, *Theory of elasticity of an anisotropic body,* Holden-Day, San Francisco, USA (1963).

[19] A. K. Kaw, *Mechanics of Composite Materials,* CRC Press, Boca Raton (2006).

[20] Q. H. Qin, General solutions for thermopiezoelectrics with various holes under thermal loading, *International Journal of Solids and Structures*, 37 (39) (2000) 5561-5578.

[21] Q. H. Qin and Y. W. Mai, Crack growth prediction of an inclined crack in a half-plane thermopiezoelectric solid, *Theoretical and Applied Fracture Mechanics*, 26 (3) (1997) 185-191.

[22] H. Wang and Q. H. Qin, A new special element for stress concentration analysis of a plate with elliptical holes, *Acta Mechanica*, 223 (2012) 1323-1340.

[23] Q. H. Qin and H. Wang, *MATLAB and C Programming for Trefftz Finite Element Methods,* CRC Press, Boca Raton (2009).

[24] S. M. Chern and M. E. Tuttle, On displacement fields in orthotropic laminates containing an elliptical hole, *Journal of Applied Mechanics*, 67 (3) (2000) 527-539.

[25] D. T. Reilly and A. H. Burstein, The elastic and ultimate properties of compact bone tissue, *Journal of Biomechanics*, 8 (6) (1975) 393-405.

Appendix

A.1 Analytical solution of anisotropic cantilever beam under uniform pressure

Under the assumption

$$u_1\big|_{X_1=l,X_2=0}=0,\quad u_2\big|_{X_1=l,X_2=0}=0,\quad \left.\frac{\partial u_2}{\partial X_1}\right|_{X_1=l,X_2=0}=0$$

the displacement and stress components can be derived by Lekhniskii anisotropic potential theory as

$$\begin{aligned}
u_1 = & -\frac{qs_{12}}{2h}X_1-\frac{qs_{16}}{4hb}X_1^{\,2}-\frac{2qs_{11}}{hb^3}X_1^{\,3}X_2-\frac{3qs_{16}}{hb^3}X_1^{\,2}X_2^{\,2} \\
& +\frac{q}{hb}\left(\frac{9s_{12}}{10}-\frac{3s_{66}}{10}+\frac{s_{16}^2}{5s_{11}}\right)X_1X_2+\frac{2q}{hb^3}\left(s_{12}+s_{66}-\frac{2s_{16}^2}{s_{11}}\right)X_1X_2^{\,3} \\
& -\frac{q}{2hb}\left(\frac{8s_{12}s_{16}}{5s_{11}}+\frac{13s_{16}s_{66}}{10s_{11}}-\frac{6s_{16}^3}{5s_{11}^2}-3s_{26}\right)X_2^{\,2} \\
& -\frac{q}{2hb^3}\left(-\frac{4s_{12}s_{16}}{s_{11}}-\frac{3s_{16}s_{66}}{s_{11}}+\frac{4s_{16}^3}{s_{11}^2}+2s_{26}\right)X_2^{\,4} \\
& +\frac{ql}{10hb^3}\left(20l^2s_{11}-9b^2s_{12}+3b^2s_{66}-2b^2\frac{s_{16}^2}{s_{11}}\right)X_2+\frac{ql}{4hb}\left(2bs_{12}+ls_{16}\right) \\
u_2 = & -\frac{qs_{26}}{2h}X_1-\frac{ql}{10hb^3}\left(20l^2s_{11}-9b^2s_{12}+3b^2s_{66}-2b^2\frac{s_{16}^2}{s_{11}}\right)X_1 \\
& -\frac{q}{2hb}\left(\frac{9s_{12}}{10}+\frac{6s_{66}}{5}-\frac{4s_{16}^2}{5s_{11}}\right)X_1^{\,2}+\frac{qs_{11}}{2hb^3}X_1^{\,4}-\frac{3qs_{12}}{hb^3}X_1^{\,2}X_2^{\,2} \\
& +\frac{q}{hb}\left(\frac{s_{12}s_{16}}{s_{11}}-\frac{3s_{26}}{2}\right)X_1X_2-\frac{2q}{hb^3}\left(\frac{2s_{12}s_{16}}{s_{11}}-s_{26}\right)X_1X_2^{\,3}-\frac{qs_{22}}{2h}X_2 \\
& -\frac{q}{2hb}\left(\frac{3s_{12}^2}{5s_{11}}+\frac{3s_{12}s_{66}}{10s_{11}}-\frac{6s_{12}s_{16}^2}{5s_{11}^2}-\frac{3s_{22}}{2}+\frac{s_{16}s_{26}}{s_{11}}\right)X_2^{\,2} \\
& +\frac{q}{2hb^3}\left(\frac{2s_{12}^2}{s_{11}}+\frac{s_{12}s_{66}}{s_{11}}-\frac{4s_{12}s_{16}^2}{s_{11}^2}-s_{22}+\frac{2s_{16}s_{26}}{s_{11}}\right)X_2^{\,4} \\
& +\frac{ql}{20hb^3}\left(30l^3s_{11}-9lb^2s_{12}+18lb^2s_{66}-12lb^2\frac{s_{16}^2}{s_{11}}+10b^3s_{26}\right) \\
\sigma_{11} = & -\frac{qX_1^{\,2}X_2}{2I}+\frac{q}{h}\left[\frac{s_{16}}{s_{11}}\frac{X_1}{b}\left(1-12\frac{X_2^{\,2}}{b^2}\right)+2\left(\frac{2s_{12}+s_{66}}{4s_{11}}-\frac{s_{16}^2}{s_{11}^2}\right)\left(\frac{4X_2^{\,3}}{b^3}-\frac{3X_2}{5b}\right)\right] \\
\sigma_{22} = & \frac{q}{2h}\left(-1+3\frac{X_2}{b}-4\frac{X_2^{\,3}}{b^3}\right) \\
\sigma_{12} = & -\frac{qX_1}{2I}\left(\frac{b^2}{4}-X_2^{\,2}\right)-\frac{q}{h}\frac{s_{16}}{s_{11}}\left(\frac{y}{b}-\frac{4X_2^{\,3}}{b^3}\right)
\end{aligned}$$

in which $I=hb^3/12$.

Qinghua Qin, born in 1958, is a Professor in Research School of Engineering, Australian National University. He has been researching on computational engineering, additive menufacturing, nanomechanics and mechanics of metamaterials.